



HAL
open science

Ultrafast sunlight-induced polymerization: Unveiling 2phenylnaphtho[2,3-d]thiazole-4,9-dione as a unique scaffold for high-speed and precision 3D printing

Ji Feng, Yijun Zhang, Fabrice Morlet-Savary, Michael Schmitt, Jing Zhang, Pu Xiao, Frédéric Dumur, Jacques Lalevée

► To cite this version:

Ji Feng, Yijun Zhang, Fabrice Morlet-Savary, Michael Schmitt, Jing Zhang, et al.. Ultrafast sunlight-induced polymerization: Unveiling 2phenylnaphtho[2,3-d]thiazole-4,9-dione as a unique scaffold for high-speed and precision 3D printing. *Small*, 2024, 20 (32), pp.2400230. 10.1002/smll.202400230 . hal-04670097

HAL Id: hal-04670097

<https://hal.science/hal-04670097v1>

Submitted on 11 Aug 2024

HAL is a multi-disciplinary open access archive for the deposit and dissemination of scientific research documents, whether they are published or not. The documents may come from teaching and research institutions in France or abroad, or from public or private research centers.

L'archive ouverte pluridisciplinaire **HAL**, est destinée au dépôt et à la diffusion de documents scientifiques de niveau recherche, publiés ou non, émanant des établissements d'enseignement et de recherche français ou étrangers, des laboratoires publics ou privés.

1 **Ultrafast sunlight-induced polymerization: Unveiling 2-**
2 **phenyl naphtho[2,3-*d*]thiazole-4,9-dione as a unique scaffold**
3 **for high-speed and precision 3D printing**

4
5 **Ji Feng ^{a,b}, Yijun Zhang ^{a,b}, Fabrice Morlet-Savary ^{a,b}, Michael Schmitt ^{a,b}, Jing**
6 **Zhang ^c, Pu Xiao ^{d*}, Frédéric Dumur ^{e*}, and Jacques Lalevée ^{a,b*}**

7
8 ^a Université de Haute-Alsace, CNRS, IS2M UMR7361, F-68100 Mulhouse, France.

9 ^b Université de Strasbourg, France.

10 ^c Future Industries Institute, University of South Australia, Mawson Lakes, SA 5095,
11 Australia.

12 ^d State Key Laboratory of High Performance Ceramics and Superfine Microstructure,
13 Shanghai Institute of Ceramics, Chinese Academy of Sciences, Shanghai 200050, P.
14 R. China.

15 ^e Aix Marseille Univ, CNRS, ICR, UMR 7273, F-13397 Marseille, France.

16
17 E-mail address: jacques.lalevee@uha.fr (J. L.); frederic.dumur@univ-amu.fr (F.D.);

18 p.xiao@mail.sic.ac.cn (P.X.)

19
20
21
22 **Abstract:** A series of 15 novel dyes based on the 2-phenyl naphtho[2,3-*d*]thiazole-4,9-
23 dione scaffold and one compound based on the 2,3-diphenyl-1,2,3,4-
24 tetrahydrobenzo[*g*]quinoxaline-5,10-dione scaffold are synthesized and studied as
25 photoinitiators. These compounds are used in two- and three-component high-
26 performance photoinitiating systems for the free radical polymerization of
27 trimethylolpropane triacrylate (TMPTA) and polyethylene glycol diacrylate (PEGDA)
28 under natural sunlight conditions. Remarkably, the conversion of TMPTA can reach
29 ~60% within a mere 20 seconds, while PEGDA attains a 96% conversion within 90
30 seconds. To delve into the intricate chemical mechanisms governing free radical
31 polymerization, an array of analytical techniques is employed. Specifically, UV-visible
32 absorption and fluorescence emission spectra, steady-state photolysis experiments,
33 stability experiments, fluorescence quenching experiments, cyclic voltammetry, and

34 electron spin resonance spin trapping (ESR-ST) experiments, collectively contribute to
35 a comprehensive understanding of the photochemical mechanisms. In addition, the
36 photoinitiation capacities of these diverse systems are determined using Real Time
37 Fourier Transformed Infrared Spectroscopy (RT-FTIR). Of particular interest is the
38 revelation that, owing to the superior initiation ability of the various dyes, high-
39 resolution 3D patterns can be successfully manufactured by direct laser write (DLW)
40 technology and 3D printing. This underscores the efficient initiation of free radical
41 polymerization processes by the newly developed dyes under both artificial and natural
42 light sources, presenting an avenue for energy-saving and environmentally friendly
43 polymerization conditions.

44

45 **Keywords:** Sunlight-induced polymerization; Naphthoquinone; photoinitiators; 2-
46 Phenyl naphtho[2,3-*d*]thiazole-4,9-dione; 3D printing.

47

48 **1. Introduction**

49 In recent years, the application of photopolymerization has witnessed a significant
50 expansion, both in industrial production and academic research. This surge can be
51 attributed to the myriad advantages of photopolymerization, encompassing its
52 environmentally friendly nature, absence of organic solvents, and safe operational
53 conditions when employing visible light [1, 2]. With the evolution of LED technology,
54 energy-efficient conditions have further become applicable to photopolymerization
55 processes. The versatility of photopolymerization technology is exemplified in its
56 applications, spanning 3D printing, biomedical materials development, coatings,
57 dentistry, and various other applications [3-10].

58 Among the diverse photopolymerization techniques, free radical polymerization
59 (FRP) stands out as one of the most prevalent and important technologies [11, 12],
60 offering mild reaction conditions, high monomer conversions, and rapid polymerization
61 rates. The efficacy of FRP processes is closely tied to the properties of the employed
62 photoinitiators (PIs). Over the years, various photoinitiators have been explored to

63 enhance their performance across visible range. The pivotal factor in
64 photopolymerization revolves around the ability of the photoinitiator/photosensitizer to
65 efficiently interact with the light source [13, 14]. The initiation process hinges on the
66 light absorption capacity of the photoinitiating systems that is governed by the molar
67 extinction coefficients of the PIs. Additionally, the absorption maximum plays a crucial
68 role in determining the excitation wavelength of a chromophore, influencing the
69 efficacy of the electron or energy transfer from the photosensitizer to the different
70 additives within the photocurable resin [15]. Up to now, common irradiation
71 wavelengths have resided in the ultraviolet (UV) (< 400 nm) and UV-visible (405 nm,
72 415 nm, etc.) range [16, 17]. However, the most optimal light source remains sunlight,
73 presenting a renewable and free energy option for photopolymerization. Similar to
74 photosynthesis in plants [15], direct photopolymerization under natural sunlight is now
75 a focal point of intense research efforts.

76 Sunlight, as a rich and sustainable energy source, remains inexhaustible as long as
77 the sun shines. Consequently, the development of sunlight-induced reactions holds a
78 prominent position in contemporary [18], encompassing areas such as CO₂ conversion
79 and decomposition [19, 20]. Another critical consideration in photopolymerization is
80 the photoinitiator itself, posing challenges in the development of efficient
81 photoinitiators suitable for sunlight-induced reactions [21]. Unlike artificial light
82 sources, sunlight exhibits lower intensity than LEDs, accompanied by a much wider
83 emission spectrum [22]. This distinction renders many photoinitiating systems, easily
84 activated with LEDs, ineffective in initiating polymerization under sunlight [23]. Even
85 in instances where polymerization can be initiated under sunlight, the process often
86 extends over several hours, with reduced monomer conversions compared to LED-
87 initiated polymerization [3]. Our previous research has identified many dyes with
88 excellent photoinitiation performance when used in multicomponent systems[24, 25];
89 however most of these were limited to LED activation. Thus, the development of dyes
90 capable of efficiently initiating polymerization processes under sunlight assumes
91 paramount significance.

92 This study introduced 15 dyes based on the 2-phenylnaphtho[2,3-*d*]thiazole-4,9-
93 dione scaffold and 1 dye based on 2,3-diphenyl-1,2,3,4-
94 tetrahydrobenzo[*g*]quinoxaline-5,10-dione, hitherto unreported in the literature. These
95 dyes exhibited outstanding photoinitiation abilities under UV-visible light (e.g.
96 LED@405 nm and LED@450 nm). Notably, five of the dyes exhibited the exceptional
97 photoinitiating ability under sunlight, enabling rapid resin curing within one minute of
98 exposure. The achieved monomer conversions, obtained at low photoinitiator/additive
99 content and short exposure time (RT-FTIR profiles), represented an unprecedented
100 advancement in the field. The elucidation of the photochemical mechanisms governing
101 the polymerization process involved a comprehensive analysis of light absorption and
102 fluorescence characteristics, cyclic voltammetry and ESR-ST experiments. The
103 findings culminated in the successful application of several formulations exhibiting
104 excellent photoinitiation abilities in DLW and 3D printing, yielding clear and precise
105 3D patterns. Leveraging the remarkable performance in outdoor sunlight
106 polymerization and applications in 3D printing, the dyes based on 2-
107 phenylnaphtho[2,3-*d*]thiazole-4,9-dione scaffold have emerged as promising
108 candidates for green polymer synthesis and large-scale outdoor applications.

109 **2. Experimental Process**

110 **2.1 Dyes and other materials.**

111 A collection of 16 dyes used for photopolymerization (under UV-visible light and
112 under sunlight in the air) were successfully synthesized. Chemical structures are shown
113 in Figure 1, and the synthetic routes used to prepare these compounds are detailed in
114 the following Section 3.1 and in supporting information. The different monomers i.e.
115 TMPTA and PEGDA (average M_n 575g/mol) were all purchased from Sartomer
116 (France). The benchmark commercial photoinitiator 2-isopropylthioxanthone (ITX)
117 used for comparison was obtained from Sartomer-Lambson (United Kingdom). Ethyl
118 4-dimethylaminobenzoate (EDB) used as the electron donor and *bis*(4-*tert*-
119 butylphenyl)iodonium hexafluorophosphate (Iod) as the electron acceptor were
120 purchased from Sartomer-Lambson (United Kingdom) (See Figure S1).

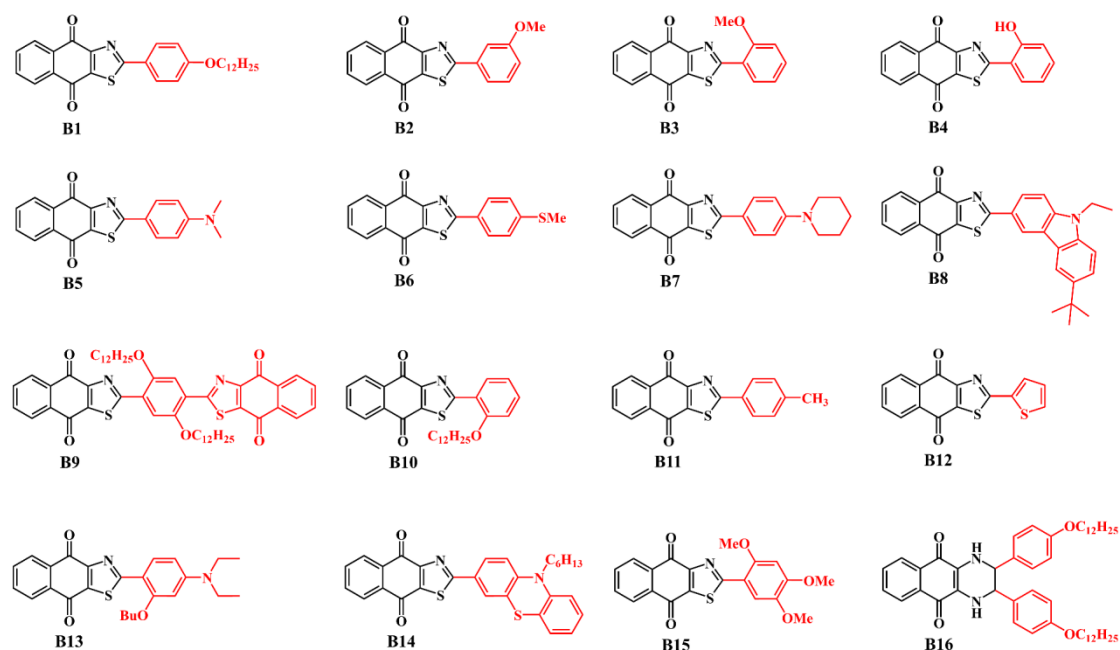


Figure 1. Chemical structures of dyes B1-B16.

2.2 UV-visible absorption and fluorescence properties of Dyes.

The UV-visible absorption properties and UV steady-state photolysis of the sixteen dyes, dissolved in dichloromethane at a concentration of 5×10^{-5} M, were studied using a JASCO V730 spectrophotometer. Steady-state photolysis of the different systems (dye, dye/EDB, dye/Iod, dye/EDB/Iod) were investigated upon irradiation (e.g. under LED@405 nm). Maintaining the consistent dye concentration in dichloromethane, fluorescence spectra of the different dyes were measured using the JASCO FP-6200 fluorescence spectrophotometer, and the fluorescence excited state lifetimes were determined using the HORIBA PPD-850 fluorimeter.

Fluorescence quenching experiments were performed using the JASCO FP-6200 spectrofluorometer, allowing for the extraction of pertinent parameters such as the electron transfer quantum yields (ϕ_{et}) using equation (1). The Stern-Volmer coefficients (K_{sv}) correspond to the slopes of the Stern-Volmer treatment in the fluorescence quenching experiments.

$$\phi_{et} = \frac{K_{sv}[\text{additive}]}{1+K_{sv}[\text{additive}]} \quad (1)$$

140

141 **2.3 Free radical photopolymerization (FRP) under near UV/visible-light**
142 **irradiation and sunlight-induced polymerization under air.**

143 The different formulations used for photopolymerization were prepared as follows:
144 dye/EDB (two-component) and dye/EDB/Iod (three-component) were mixed and
145 dissolved into TMPTA, and then stirred overnight in the dark. The weight content of
146 dye, EDB and Iod were calculated based on the weight of the monomer, and the
147 influence of the different weight content ratio of each component on the
148 photopolymerization efficiency were investigated. After that, the prepared formulations
149 were subjected to photopolymerization experiments of thick and thin samples, and the
150 specific operations were as follows: one drop of the prepared resin was dropped
151 between two polypropylene films (for thickness from 10 to 100 microns) for thin
152 samples, and five drops of the prepared resins were dropped into a plastic mold (2 mm)
153 for thick samples. Then, the characteristic peaks of acrylate functional groups were
154 continuously detected at about 6150 cm^{-1} (2 mm thick sample) and 1650 cm^{-1} (thin
155 sample 10 to 100 microns) by RT-FTIR (JASCO FTIR-4700). The acrylate conversions
156 were obtained by the following equation:

157 $Conversion (\%) = \left(1 - \frac{A_t}{A_0}\right) \times 100\%$ (2)

158 where A_0 is the initial peak area before light irradiation and A_t is the peak area
159 after being irradiated with light for t s.

160 In addition to the polymerization experiments conducted under artificial light
161 sources, we explored sunlight-induced photopolymerization using the same
162 formulations as described earlier. The sunlight-induced polymerization experiment was
163 carried out on August 22, 2023, from 1 pm to 3 pm, aligning with French time. The
164 experiment site was in Mulhouse (+77 43 ' E, 47 75 ' N), France, where the weather
165 conditions were sunny. The conversions of the acrylate functional groups were
166 monitored by RT-FTIR spectroscopy.

167 **2.4 Redox potentials of dyes obtained by cyclic voltammetry.**

168 Redox potentials of the dyes were measured using cyclic voltammetry. The

169 specific operation was that the dyes and the supporting electrolyte
170 (tetrabutylammonium hexafluorophosphate) were dissolved in dichloromethane, and
171 the redox potentials of the dyes were measured under nitrogen atmosphere. Equations
172 (3) and (4) were used to calculate the change of free energy ($\Delta G^{S^1}_{EDB}$ or $\Delta G^{S^1}_{Iod}$) from
173 the excited singlet states in the electron transfer reaction between the dyes and the
174 additives. The singlet excited state energy level (E_{S^1}) of the dyes was determined from
175 the intersection of the normalized UV-visible absorption and fluorescence spectra.
176 Finally, the oxidation potential of EDB is 1.0 V and the reduction potential of the
177 iodonium salt (Iod) is -0.7 V, as reported in the literature [26, 27].

178

$$179 \Delta G^{S^1}_{Iod} = E_{ox} - (-0.7) - E_{S^1} \quad (3)$$

$$180 \Delta G^{S^1}_{EDB} = 1 - E_{red} - E_{S^1} \quad (4)$$

181

182 **2.5 Electron Spin Resonance – Spin Trapping (ESR-ST) experiments.**

183 ESR-ST experiments were carried out with the ESR X-band spectrometer (Bruker
184 EMX-plus) to study the free radicals generated under the LED@405 nm irradiation.
185 Under nitrogen atmosphere, free radicals were captured by phenyl-*N-tert*-butylnitrone
186 (PBN). The concentration of PBN was $\sim 5 \times 10^{-4}$ M. All operations were carried out at
187 room temperature. In addition, ESR-ST spectra were simulated by PEST WINSIM
188 program.

189 **2.6 Application of 3D printing experiments.**

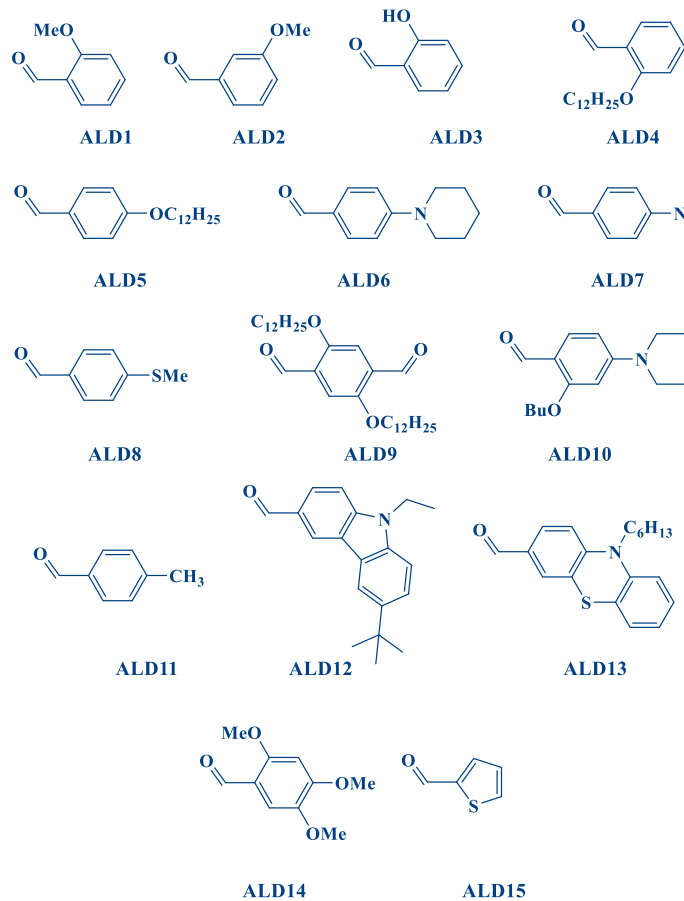
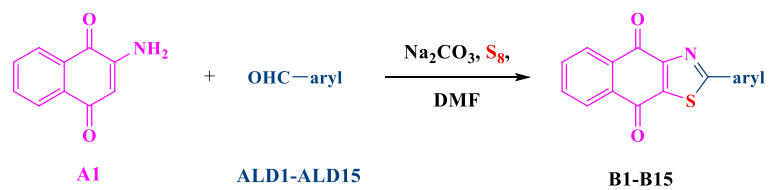
190 The formulations with good photopolymerization performance were selected for
191 3D printing experiments. First of all, a two-component system (0.1wt% dye/1wt% EDB,
192 TMPTA as the monomer) was used to conduct the direct laser write (DLW) experiments
193 with a computer-programmed x,y desk with a mounted laser diode at 405 nm, in which
194 the glass tank (3 cm in length, 2 cm in width, and 0.3 cm in height) for printing was
195 made by ourselves. Furthermore, a three-component system (0.1wt% dye/1wt%
196 EDB/1wt% Iod, TMPTA as the monomer) was used to print 3D objects with a Digital
197 Light Processing (DLP) 3D Printer (Anycubic Photon D2, China), and the thickness of
198 the layer was controlled at 0.02 mm. The printed patterns were observed by Scanning

199 Electron Microscope (SEM) and Numerical Optical Microscope (DSX-HRSU from
200 Olympus Corporation).

201 **3. Results and Discussion**

202 **3.1 Synthesis of the dyes.**

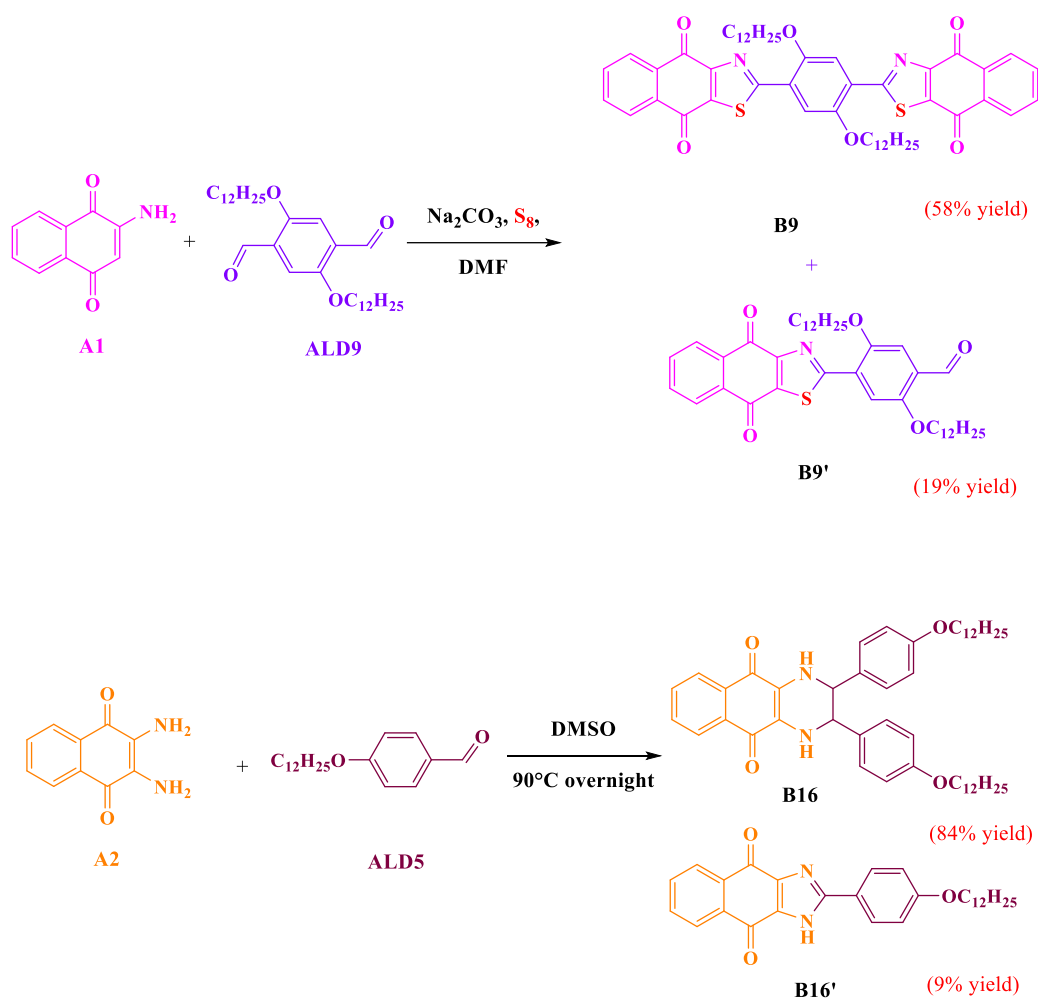
203 B1-B15 were prepared in one step starting from 2-aminonaphthalene-1,4-dione A1
204 and the appropriate aldehyde ALD1-ALD15 using the synthetic route as reported
205 previously [28] (See Scheme 1). With this method, all dyes could be obtained with the
206 reaction yields ranging between 58% yield for B9 and 92% yield for B10 after
207 purification/isolation (See Table 1). It has to be noticed that all dyes exhibited a D- π -A
208 structure (with D and A standing for donor and acceptor respectively) except for B9 that
209 A- π -D- π -A was found. To access to this structure, 2,5-
210 *bis*(dodecyloxy)terephthalaldehyde ALD9 was used as the dialdehyde (See Scheme 2).
211 Among the series of dyes, the lowest reaction yield (58%) was obtained during the
212 synthesis of this dye, 4-(4,9-dioxo-4,9-dihydronaphtho[2,3-*d*]thiazol-2-yl)-2,5-
213 *bis*(dodecyloxy)benzaldehyde B9' being isolated as the side product of this reaction in
214 19% yield. A different synthesis was used for B16. Starting from 2,3-
215 diamionaphthalene-1,4-dione A2 and two equivalents of 4-(dodecyloxy)benzaldehyde,
216 B16 could be identified as the main product of the reaction and isolated in 84% yield.
217 As a side product of this second reaction, 2-(4-(dodecyloxy)phenyl)-1*H*-naphtho[2,3-
218 *d*]imidazole-4,9-dione B16' could be obtained in 9% yield (See Scheme 2). It has to be
219 noticed that the synthetic route used to produce B16 was first reported in 1987 and the
220 synthesis of such compounds has never been revisited since this pioneering work [29].



221

222

Scheme 1. Synthetic routes to B1-B15.



223

224

Scheme 2. Synthetic routes to B9 and B16.

225

226

Table 1. Reaction total yields obtained during the synthesis of B1-B16.

Compounds	Reaction yields (%)	Compounds	Reaction yields (%)
B1	81	B9	58
B2	77	B10	92
B3	89	B11	81
B4	80	B12	88
B5	67	B13	65
B6	88	B14	85
B7	88	B15	85
B8	91	B16	84

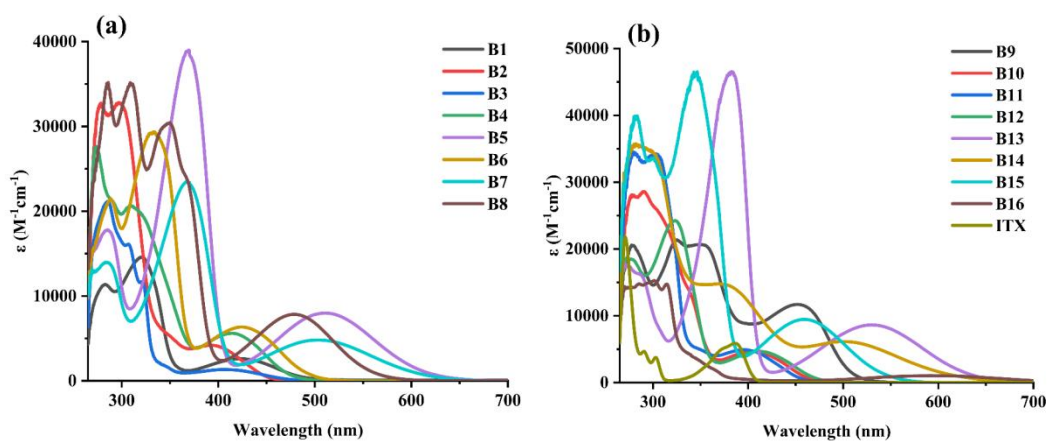
227

228 3.2 Light absorption properties of the different dyes.

229 UV-visible absorption spectra of the 16 dyes and the commercial photoinitiator 2-

230 isopropylthioxanthone (ITX) dissolved in dichloromethane were recorded and the

231 results are shown in Figure 2. Light absorption characteristics of the different dyes are
 232 summarized in Table 2. Figure 2 vividly illustrates robust absorption peaks in the UV-
 233 visible region for all dyes, assigned to $\pi \rightarrow \pi^*$ transitions [30]. Notably, the maximum
 234 absorption peaks of B1, B2, B3, B4, B10, B11, and B12 were around 405 nm, which
 235 were therefore highly favorable for photopolymerization experiments conducted under
 236 the LED@405 nm and a benchmark in 3D printing (See Section 3.3). The maximum
 237 absorption wavelengths (λ_{\max}) of B1, B2, B3, B10, and B11 were 420, 400, 410, 410,
 238 and 400 nm, respectively. Correspondingly, their molar extinction coefficients (ϵ_{\max}) at
 239 λ_{\max} were 2610, 4170, 1320, 4690, and 4920 $\text{M}^{-1} \cdot \text{cm}^{-1}$, respectively. In addition, the
 240 molar extinction coefficients ($\epsilon_{405\text{nm}}$) at $\lambda_{405\text{nm}}$ were 2310, 3870, 1320, 4690, and 4730
 241 $\text{M}^{-1} \cdot \text{cm}^{-1}$, respectively. These five dyes demonstrated excellent photoinitiation abilities,
 242 and the results presented in Section 3.3 also confirmed their high photoinitiation
 243 performance as photoinitiators in free radical polymerization when 2 mm thick resin
 244 samples in open molds (no protection against oxygen inhibition) were exposed to
 245 sunlight outdoors (clear sky conditions). Contrastingly, B5, B7-B9, and B13-B16
 246 showed strong absorption peaks in the 450-600 nm range, which may be due to a
 247 redshift of the $\pi \rightarrow \pi^*$ transition with an increase of the electronic density, resulting from
 248 the presence of strong electron-donating groups. However, these dyes exhibited poor
 249 photoinitiation abilities [30], as elaborated in Section 3.3.



250
 251 **Figure 2.** UV-visible absorption spectra of dyes in dichloromethane. (a) B1-B8, (b)
 252 B9-B16 and ITX.
 253

254 **Table 2.** Light absorption characteristics of the dyes (λ_{\max} for the red shifted
 255 transitions)

PIs	λ_{\max} (nm)	ϵ_{\max} ($M^{-1}.cm^{-1}$)	ϵ_{405} ($M^{-1}.cm^{-1}$)	moiety
B1	420	2610	2310	4-dodecyloxyphenyl
B2	400	4170	3870	3-methoxyphenyl
B3	410	1320	1320	2-methoxyphenyl
B4	410	5600	5410	2-hydroxyphenyl
B5	510	7990	4110	4-dimethylaminophenyl
B6	430	6340	5630	4-methylthiophenyl
B7	510	4810	4570	4-piperidinylphenyl
B8	480	7830	2400	<i>tert</i> -butyl-(<i>N</i> -ethyl)carbazolyl
B9	450	11690	8760	naphthothiazolodione- <i>bis</i> (dodecyloxy)phenylene
B10	410	4690	4690	2-dodecyloxyphenyl
B11	400	4920	4730	<i>p</i> -tolyl
B12	410	4660	4570	thiophenyl
B13	530	8630	12120	2-butoxy-4-(diethylamino)phenyl
B14	500	6130	11240	<i>N</i> -hexyl-phenothiazinyl
B15	460	9460	4530	2,4,5-trimethoxyphenyl
B16	590	1220	420	<i>bis</i> (<i>p</i> -dodecyloxy)phenyl
ITX	390	5890	1000	

256

257 **3.3 Photopolymerization kinetics with the dyes in two or three-component**
 258 **photoinitiating systems under LED@405 nm, 450 nm, and sunlight.**

259 To investigate the photoinitiation ability of the fifteen dyes based on the 2-
 260 phenyl-naphtho[2,3-*d*]thiazole-4,9-dione scaffold and the one dye based on the 2,3-
 261 diphenyl-1,2,3,4-tetrahydrobenzo[*g*]quinoxaline-5,10-dione scaffold,
 262 photopolymerization were carried out under LED@405 nm, LED@450 nm, and
 263 sunlight exposure. The photoinitiation ability of two different two-component
 264 (dye/EDB and dye/Iod) systems and one three-component (dye/EDB/Iod) system were
 265 studied to clarify the influence of co-initiators (EDB as the electron/hydrogen donor and
 266 Iod as the electron acceptor) on the polymerization kinetics of TMPTA. The
 267 conversions of acrylate functional groups were determined using the RT-FTIR at room
 268 temperature. Specifically, for the blank groups shown in Figure S2 (i.e. dye alone, EDB
 269 alone, and Iod alone), no polymerization or poor photoinitiation abilities were
 270 determined, evidencing that the two co-initiators EDB and Iod may only play a crucial
 271 role in the initiation step once combined with the dyes.

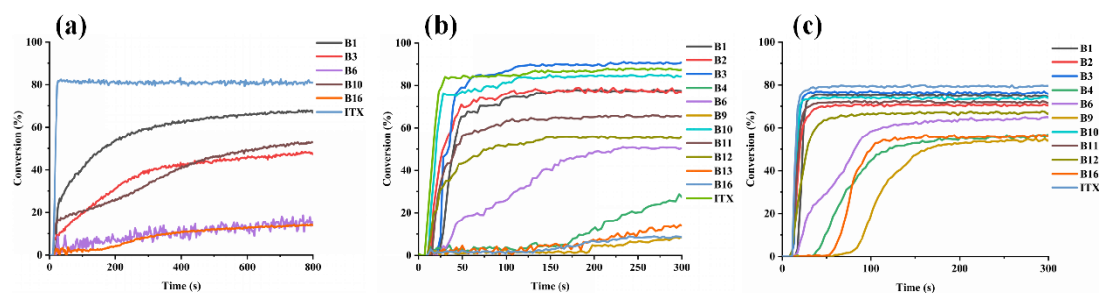
272 Polymerization profiles obtained with the two-component dye/EDB systems are

273 shown in Figure S3 (thick sample) and Figure S4 (thin sample), while the final acrylate
274 function conversions (FCs) are listed in Table S1 (thick sample) and Table S2 (thin
275 sample). Influence of the dye concentrations on the polymerization performance of
276 TMPTA was also investigated. Specifically, for the two-component dye/EDB system,
277 EDB concentration was fixed to 1 wt%. When the dye concentration was set to 0.1 wt%,
278 the conversions of thick samples (See Figure S3(c)) and thin samples (See Figure S4(c))
279 were optimal, especially for thick samples containing B1 and B10 and thin sample
280 containing B16. The conversions of thick samples were close to 80%, while it can reach
281 90% for the thin samples. It implied that when the dye concentrations were 1 wt%, the
282 solubility of the dyes in TMPTA was low and the precipitation can be clearly seen in
283 the different formulations, which led to a poor light penetration i.e. inner filter effect
284 due to the high light absorption properties of the dyes. By decreasing the dye
285 concentrations, the different formulations became clearer and more transparent, which
286 can be beneficial to photopolymerization.

287 In the case of the two-component dye/Iod (1 wt%) system (See Figure S5 (thin
288 sample) and Figure S6 (thick sample)), the results were basically consistent with that
289 obtained with the two-component dye/EDB system. Considering that numerous dyes
290 exhibited good light absorption properties in the 450-550 nm range, polymerization
291 experiments were also carried out under the LED@450 nm, using the two-component
292 dye/EDB (0.1%/1% w/w) system in TMPTA, both in thick and thin samples. Excellent
293 polymerization performance could be determined, as shown in Figure S7.

294 Considering that the different dyes can form photoinitiating systems with Iod and
295 EDB, their combination in three-component dye/Iod/EDB systems was also
296 investigated. As shown in Figures 3 (a) and (b), in thick samples, when the
297 concentration of EDB and Iod in TMPTA were kept constant at 1 wt%, the dye
298 concentration of 0.1wt% furnished excellent polymerization profiles (See Figure 3 (b)).
299 The FC with B3 even reached 91%, and the conversions with B10 and B1 were around
300 80%. However, when the concentration of dyes was set to 1 wt%, the dyes were not
301 completely dissolved in TMPTA, resulting in low polymerization efficiency (again

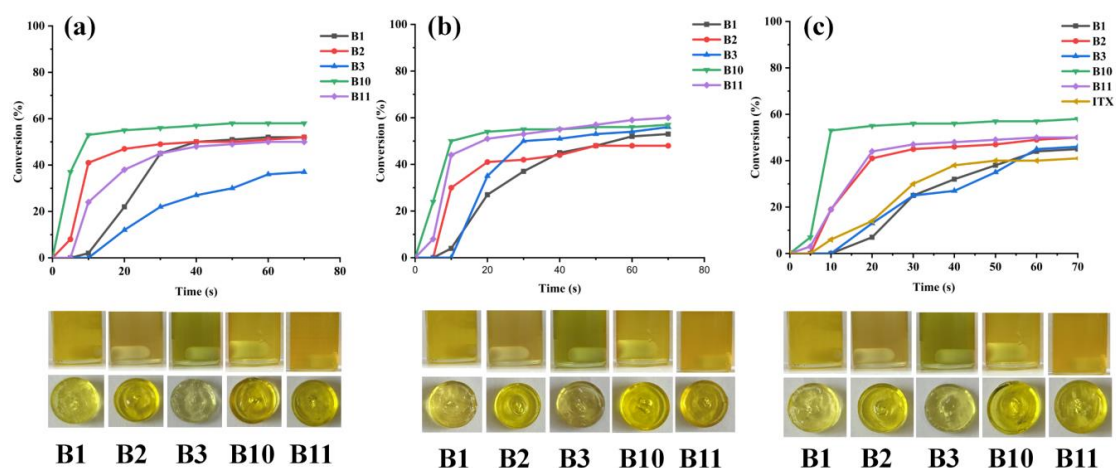
302 ascribed by an inner filter effect due to the high light absorption properties of the dyes).
 303 When the amount of EDB and Iod were reduced to 0.1 wt% (See Figure 3 (c)), the
 304 different three-component photoinitiating systems could maintain a high conversion
 305 level and all thick samples could be deeply cured (See Figure S8 and Figure S9). In the
 306 case of thin samples (See Figure S10), the higher conversions could be determined.
 307 Specifically, polymerization of TMPTA initiated with the photoinitiating systems based
 308 on B1, B2, B3, B10, and B11 was very fast, and the maximum monomer conversion
 309 could be obtained within only 20 seconds of irradiation with LED@405nm and
 310 LED@450 nm. On the contrary, other photoinitiating systems only showed poor
 311 photoinitiation abilities, which was characterized by low conversions obtained after a
 312 long induction period. As a result, B1, B2, B3, B10, and B11 were selected as the
 313 photoinitiators/photosensitizers for photopolymerization experiments done under
 314 sunlight and under air.



315
 316 **Figure 3.** Photopolymerization profiles of TMPTA for thick sample (2 mm) upon
 317 exposure to LED@405 nm irradiation. Initiated by (a) dye/EDB/Iod 1%/1%/1% w/w/w;
 318 (b) dye/EDB/Iod 0.1%/1%/1% w/w/w; (c) dye/EDB/Iod 0.1%/0.1%/0.1% w/w/w. The
 319 irradiation starts at $t = 10$ s.

320 The sunlight-induced photopolymerization were carried out at 1-4 pm on August
 321 22, 2023 in Mulhouse, France. As shown in Figure 4, three kinds of two-component
 322 and three-component systems with excellent photoinitiation abilities under artificial
 323 irradiation were selected to for the photopolymerization under sunlight (thick sample,
 324 2 mm). Interestingly, the three systems showed high performance under sunlight.
 325 Photopolymerization profiles obtained with the two-component (dye/EDB 0.1%/1%
 326 w/w) system are shown in Figure 4 (a), while those of the three-component systems are

327 presented in Figures 4 (b) and (c). All FCs are listed in Table 3. It can be seen from the
 328 three-component systems that B10 reached the over 50% functional conversion (green
 329 curve) within 10 s and compared to the other four dyes, even for the system with the
 330 low concentrations of additives (i.e., dye/EDB/Iod 0.1%/0.1%/0.1% w/w/w; Figure 4
 331 (c)). Change of the formulations before and after polymerization is also given at the
 332 bottom of Figure 4 and according to the experimental results, there were still a little
 333 liquid at the surface of the resins containing B1 and B2 after polymerization, but for
 334 resins containing B3, B10, B11, and ITX, they were completely polymerized as solids
 335 (tack-free surfaces). It can be seen that all thick samples could be deeply cured with
 336 sunlight. Based on the excellent polymerization performance of these dyes under
 337 sunlight, polymerization experiments were also carried out with the three-component
 338 (dye/EDB/Iod 0.1%/1%/1% w/w/w) system in another monomer PEGDA. As shown in
 339 Figure S11, the acrylate functional group conversion of PEGDA initiated by B10
 340 reached 96%, which was similar to that of the commercial initiator ITX. According to
 341 the above experimental results, B10 synthesized in this study has a great application
 342 prospect in inducing photopolymerization under sunlight.



343 **Figure 4.** Photopolymerization profiles of TMPTA for thick sample (2 mm) under
 344 sunlight in the air. Initiated by (a) dye/EDB 0.1%/1% w/w; (b) dye/EDB/Iod 0.1%/1%/1%
 345 w/w/w; (c) dye/EDB/Iod 0.1%/0.1%/0.1% w/w/w. (Black curve for B1, red curve for
 346 B2, blue curve for B3, green curve for B10, purple curve for B11 and yellow curve for
 347 ITX)

349

350 **Table 3.** Final acrylate function conversions (FCs) of TMPTA in the presence of dyes
 351 with co-initiators under sunlight-induced polymerization.

Two-component		Three-component		Three-component	
Dye/EDB		Dye/EDB/Iod		Dye/EDB/Iod	
(0.1%/1% w/w)		(0.1%/1%/1%)		(0.1%/0.1%/1%)	
Monomer: TMPTA		Monomer: TMPTA		Monomer: TMPTA	
Dye	FCs (%)	Dye	FCs (%)	Dye	FCs (%)
B1	52	B1	53	B1	45
B2	52	B2	48	B2	50
B3	37	B3	56	B3	46
B10	58	B10	58	B10	58
B11	50	B11	61	B11	50

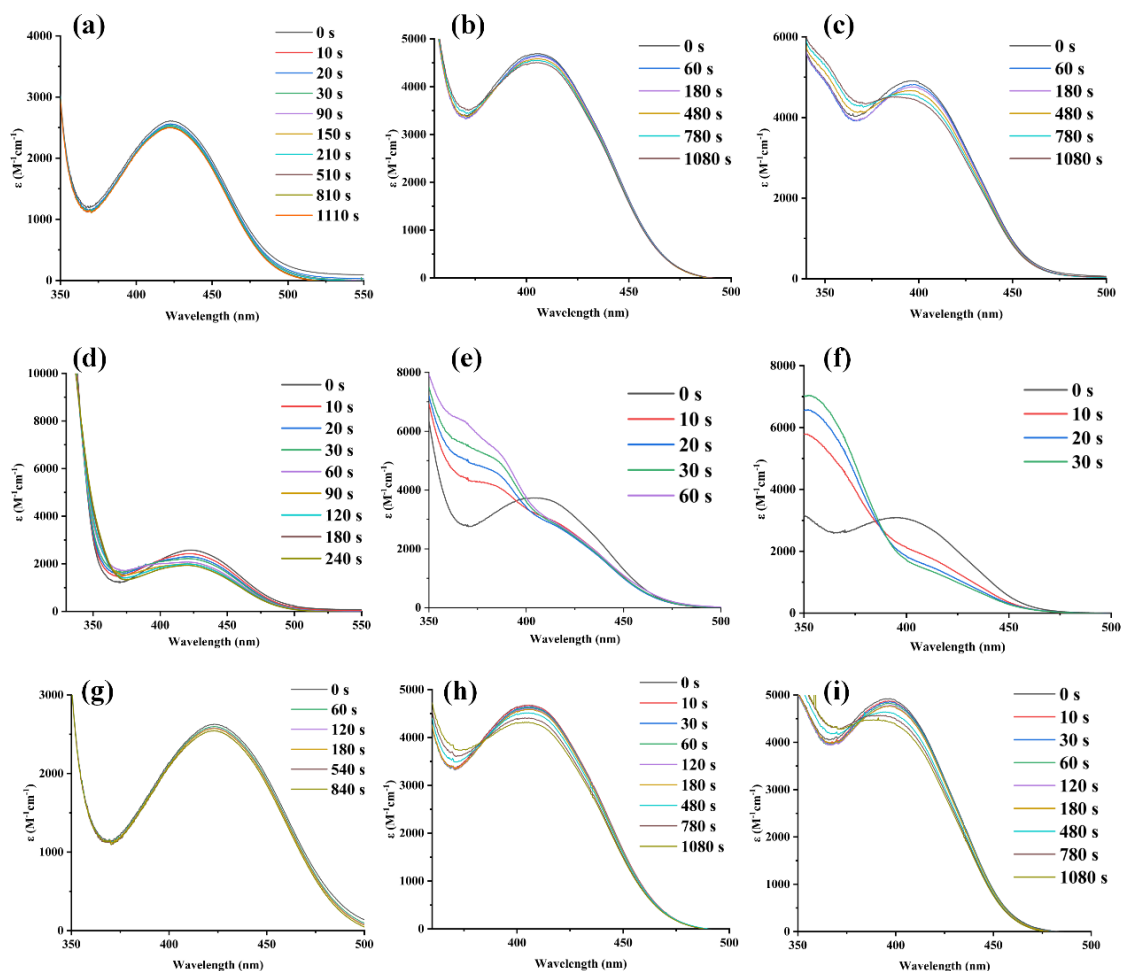
352

353 **3.4 Steady state photolysis experiments of dye, dye/EDB and dye/Iod** 354 **photoinitiation systems.**

355 To understand the interaction between the different dyes, EDB, and Iod, and to
 356 clarify the chemical mechanism involved in the photopolymerization process, steady-
 357 state photolysis experiments were carried out under the irradiation of LED@405 nm.
 358 As shown in Figure 5, the UV-visible absorption profiles of dye, dye/EDB, and dye/Iod
 359 dissolved in dichloromethane were studied respectively. The concentration was set as
 360 5×10^{-5} M for dye, 1×10^{-4} M for EDB, and 1×10^{-4} M for Iod. All the steady-state
 361 photolysis profiles are shown in Figures S12, S13 and S14.

362 As shown in Figures 5 (a), (b), and (c), the steady-state photolysis profiles of B1,
 363 B10 and B11 are presented after 18 min of irradiation with the LED@405 nm.
 364 Absorbance of the three dyes decreased slightly by elongating the irradiation time,
 365 indicating that the dyes alone were relatively stable upon the irradiation with the
 366 LED@405nm, which was in line with the photopolymerization results presented in
 367 Section 3.3. Notably, the dyes alone cannot initiate any polymerization, or the monomer
 368 conversion was low. However, in the case of the two-component dye/EDB systems, as
 369 shown in Figure 5 (d), it can be seen that the absorbance of the B1/EDB system
 370 obviously decreased within 4 min compared with the single dye system. In the case of

371 the B10/EDB system in Figure 5 (e) and B11/EDB system in Figure 5 (f), these
 372 photolysis of two two-component systems were significant within only 30 s.
 373 Interestingly, for the three two-component dye/Iod systems presented in Figures 5 (g),
 374 (h), and (i), after a long period of irradiation, the absorbance was almost the same than
 375 that of the single dye system. Obviously, the efficiency of dye/EDB combination was
 376 higher than that of dye/Iod in the photopolymerization process.



377

378 **Figure 5.** Steady-state photolysis of dye (5×10^{-5} M), EDB (1×10^{-4} M) and Iod (1×10^{-4}
 379 M) in dichloromethane under LED@405 nm. (a) dye-B1 (alone), (b) dye-B10 (alone),
 380 (c) dye-B11 (alone), (d) dye-B1 and EDB, (e) dye-B10 and EDB, (f) dye-B11 and EDB,
 381 (g) dye-B1 and Iod, (h) dye-B10 and Iod, (i) dye-B11 and Iod.

382

383 In addition, to test the stability of dyes under sunlight, steady-state photolysis
 384 experiments of B1, B2, B3, B10 and B11 were also carried out under sunlight and under

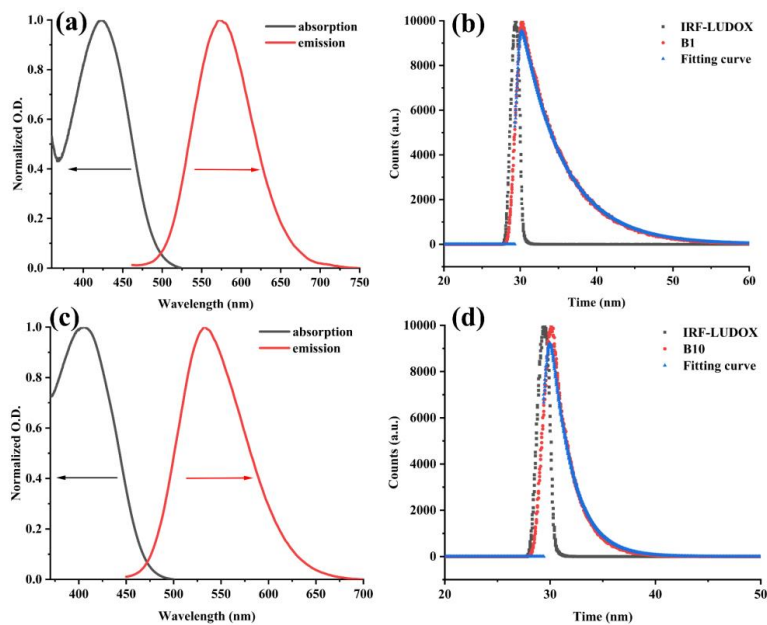
385 air. As shown in Figure S15, after a long-term sunlight irradiation, the absorbance
386 hardly changed, which proved that the dyes had a good stability under sunlight. This
387 also provides a basis for the practical application of these dyes.

388 **3.5 Fluorescence properties, fluorescence quenching experiments and chemical** 389 **mechanisms in electron transfer reaction for dyes.**

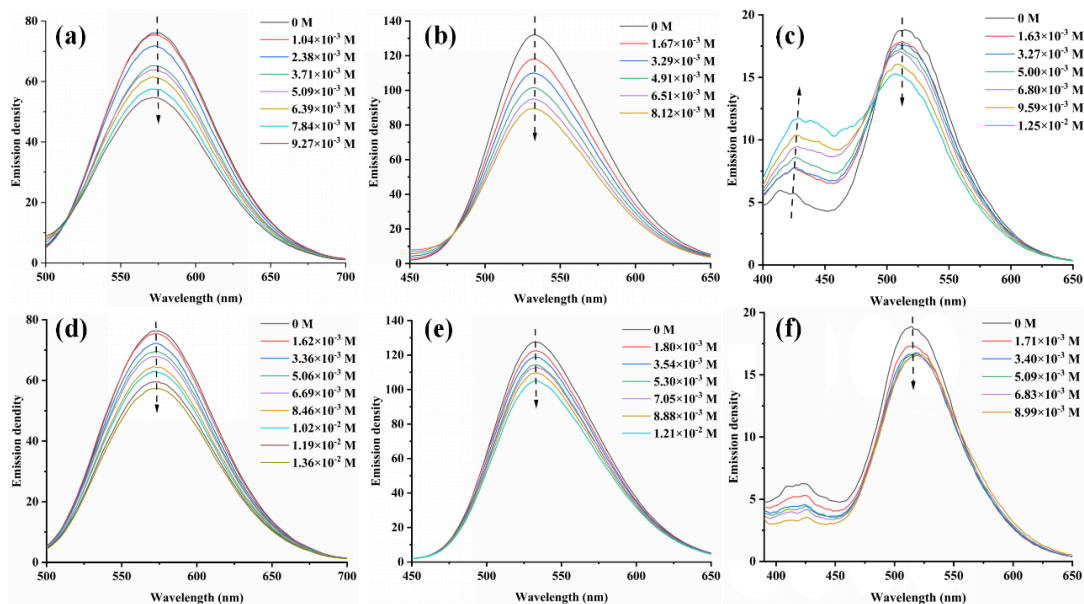
390 Fluorescence spectra of the different dyes are shown in Figure S16, and the
391 fluorescence lifetime spectra are shown in Figures 6 and S17. Fluorescence
392 characteristics of some dyes were not detected in the 200-1000 nm range due to their
393 chemical structures. Various parameters in electron transfer reaction, such as E_{S1} (See
394 Figures 6, S18 and Table 4), were obtained from the intersection of the normalized UV-
395 visible absorption and fluorescence spectra. In addition, the oxidation (E_{ox}) and
396 reduction (E_{red}) potentials of B1, B3, B10, B12, and B16 were measured by cyclic
397 voltammetry (See Figure S19), and the values of E_{ox} and E_{red} are summarized in Table
398 4. From Figure S19, the reduction peaks were clearly observed for the five investigated
399 dyes, and the oxidation peaks were only observed for B3 and B16 during the sweep
400 cycle. The Gibbs free energy change (ΔG^{S1}) of electron transfer between dyes and
401 additives (EDB and Iod) were calculated according to equations (3) and (4), and the
402 values are listed in Table 4. It can be seen from the Table that ΔG^{S1} of all dyes were
403 negative, indicating that the electron transfer reactions of dye/EDB and dye/Iod were
404 feasible.

405 Fluorescence quenching experiments of the dye/EDB systems and the dye/Iod
406 systems were also carried out in dichloromethane, as shown in Figure 7 and Figures
407 S20 and S21. For B1, B10, and B11, the addition of additives (EDB and Iod)
408 significantly decreased their fluorescence intensity. Conversely, the fluorescence
409 intensity of B11/EDB increased at 400-450 nm, which may be due to the fact that dye-
410 B11 reacted with EDB upon irradiation to generate new chromogenic substances, which
411 indicated that there was an efficient interaction between the dyes and EDB or Iod. The
412 results were consistent with the above free energy changes and steady-state photolysis
413 experiments.

414 The Stern-Volmer coefficients (K_{sv}) of dye/EDB or dye/Iod were determined by
 415 the slope of the Stern–Volmer treatment of fluorescence quenching (See Figure S22),
 416 and the electron transfer quantum yields (ϕ_{et}) (See Table 4) can be calculated by
 417 Equation 1, which was helpful for a deep understanding of the chemical mechanism in
 418 photopolymerization.



419
 420 **Figure 6.** (a) Singlet state energy of B1, (b) fluorescence decay curve of B1, (c)
 421 singlet state energy of B10, (d) fluorescence decay curve of B10.



422
 423 **Figure 7.** Fluorescence quenching of (a) dye-B1 and EDB, (b) dye-B10 and EDB, (c)
 424 dye-B11 and EDB, (d) dye-B1 and Iod, (e) dye-B10 and Iod, (f) dye-B11 and Iod in
 425 dichloromethane.

426

427 4. **Table 4.** Parameters of the chemical mechanisms associated with B1, B3, B10,
 428 B12 and B16 in dichloromethane.

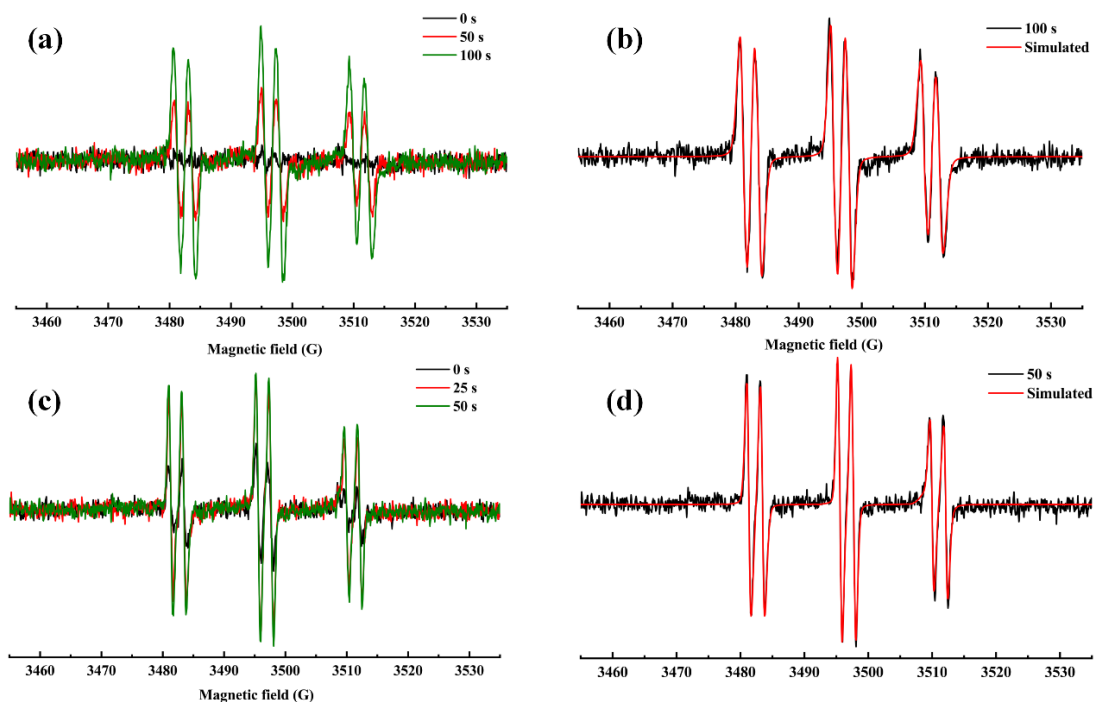
	Dye-B1	Dye-B3	Dye-B10	Dye-B12	Dye-B16
E_{ox} (V)	-	0.83	-	-	1.02
E_{red} (V)	-0.85	-1.09	-1.12	-1.04	-1.23
ΔG_{EDB}^{S1} (eV)	-0.64	-0.55	-0.51	-0.55	-0.06
ΔG_{Iod}^{S1} (eV)	-	-1.11	-	-	-0.45
E_{S1} (eV)	2.49	2.64	2.63	2.59	2.29
K_{sv} (EDB) s^{-1}	43.9	19.1	58.4	91.3	-
K_{sv} (Iod) s^{-1}	24.7	23.5	17.2	34.6	18.9
ϕ_{et} (EDB) ^a	0.69	0.49	0.74	0.82	-
ϕ_{et} (Iod) ^a	0.33	0.32	0.26	0.41	0.27

429 a : the electron transfer quantum yield is calculated from: $\phi_{et} = K_{sv} [additive] / (1 + K_{sv} [additive])$;
 430 with [additive] the EDB (0.05 M) and Iod (0.02 M) concentration.

431

432 **4.1 ESR-ST experiments.**

433 To determine the nature of the free radicals produced by the interaction between
 434 dye/EDB and dye/Iod, B1 was used as an example to successfully carry out ESR-ST
 435 experiments under the LED@405 nm (See Figure 8). As shown in Figures 8 (a) and (b),
 436 for the dye/EDB system, a free radical was successfully captured by PBN, and its
 437 hyperfine coupling constants were $\alpha_N = 14.3$ G and $\alpha_H = 2.6$ G, which may be
 438 aminoalkyl radical EDB_(-H) \cdot . In Figures 8 (c) and (d), a radical in the dye/Iod system
 439 was captured by PBN, and its hyperfine coupling constants were $\alpha_N = 14.3$ G and α_H
 440 = 2.2 G, which may be aryl radical. The results are in accordance with the experimental
 441 data reported in the literature [31].



442

443 **Figure 8.** ESR-ST spectra of the PBN radical adducts (in *tert*-butylbenzene under
 444 nitrogen atmosphere). (a) and (b) B1/EDB, (c) and (d) B1/Iod under LED@405 nm
 445 irradiation.

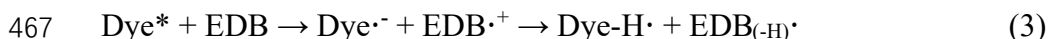
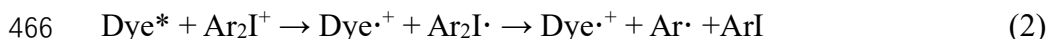
446

447 **4.2 Summary of photoinitiation mechanisms of dye.**

448 Based on the above results, the chemical mechanisms induced by the three-
 449 component photoinitiating dye/EDB/Iod system was proposed, which can be divided
 450 into three steps. The first step consisted in the excitation of the chromophore with light,
 451 enabling to promote the dye from its initial ground state to the excited state (See
 452 reaction 1). In the second step, the excited dye* reacted with Iod and EDB respectively
 453 to generate free radicals, as shown in reactions 2 and 3. Specifically, the dye* reacted
 454 with Iod to generate Ar· free radicals and dye·⁺. In addition, dye* reacted with EDB to
 455 produce EDB_(-H)· free radicals and dye-H·. In fact, the excited dye (dye*) can react with
 456 EDB and Iod separately according to a reductive and an oxidative pathway so that free
 457 radicals capable of initiating polymerization processes were produced. In a third step,
 458 Dye·⁺ produced by an oxidation reaction and Dye-H· produced by a reduction reaction
 459 can be regenerated into Dye by the interaction with EDB and Iod respectively (See
 460 reactions 4 and 5), and finally the catalytic cycle of the three-component system was

461 completed. Notably, the free radicals $\text{EDB}_{(-\text{H})}\cdot$ and $\text{Ar}\cdot$ produced during the catalytic
462 cycle were successfully detected by ESR, which provided clear evidences for the
463 proposed chemical mechanisms.

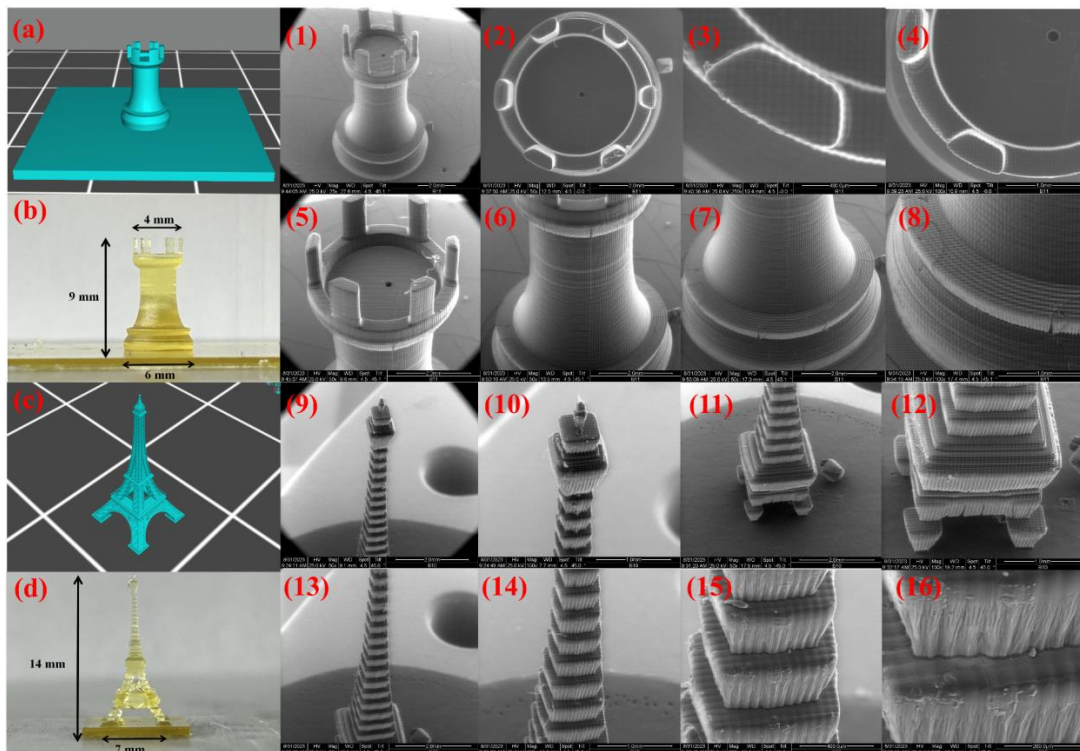
464



470

471 **4.3 Application in 3D printing**

472 Exploiting the impressive photoinitiation capabilities demonstrated by several
473 dyes in this study (efficiently initiate the FRP of TMPTA under both of LED@405 nm
474 irradiation and exposure to sunlight) we selected the two-component systems B3/EDB,
475 B10/EDB, and B12/EDB, along with the three-component systems B10/EDB/Iod and
476 B11/EDB/Iod for 3D printing. For the DLW experiments, the two-component systems
477 were employed, resulting in the rapid production of 3D letters within 2 min of
478 irradiation at 405 nm, as depicted in Figure S23. These outcomes were verified through
479 digital camera and numerical optical microscopy, highlighting the distinct and well-
480 defined outlines of printed letters. Moving to the 3D printing experiment involving the
481 three-component system, Figure 9 illustrates the successful printing of an exquisite
482 chess piece and an Eiffel tower model using a 3D printer Figures 9 (a) and (b) depict
483 the chess piece model printed by B11/EDB/Iod/TMPTA system, and Figures 9 (c) and
484 (d) showcase the Eiffel tower model printed by B10/EDB/Iod/TMPTA system. The
485 clear outline of the model is readily discernible through digital camera observation, and
486 SEM photos (See Figure 9 (1-16)) further confirm the smooth surfaces and excellent
487 spatial resolution achieved in the production of these 3D objects. These results
488 underscore the potential of the selected photoinitiating systems for high-quality and
489 precise 3D printing applications.



490

491 **Figure 9.** Digital photos of 3D printed objects. (a) and (b) dye-
 492 B11(0.1wt%)/EDB(1wt%)/Iod(1wt%)/TMPTA system; (c) and (d) dye-
 493 B10(0.1wt%)/EDB(1wt%)/Iod(1wt%)/TMPTA system; 1-8 SEM images of surface of
 494 the 3D printed objects using dye-B11/EDB/Iod/TMPTA system; 9-16 SEM images of
 495 surface of the 3D printed objects using dye-B10/EDB/Iod/TMPTA system.

496

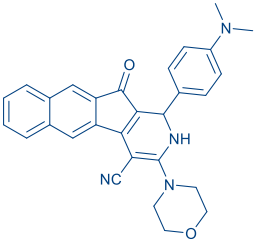
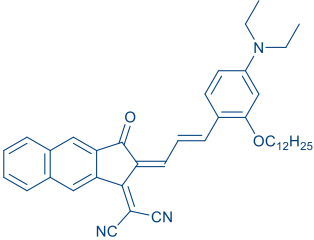
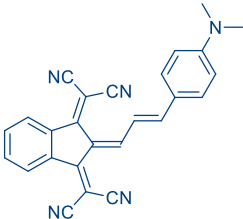
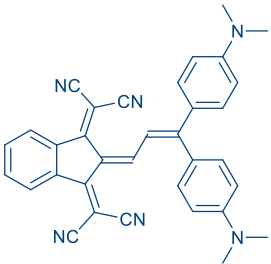
497 **4.4 Comparisons with solar photoinitiators from previous studies**

498 In Figure 4, photopolymerization profiles obtained with B1, B2, B3, B10, and B11
 499 upon sunlight irradiation in two- and three-component photoinitiating systems are
 500 presented. A thorough comparison with dyes previously reported in the literature
 501 accentuates the remarkable performance of the dyes investigated in this study. Table 5
 502 outlines the superior attributes of the identified top candidates for the FRP of TMPTA
 503 in the literature, where all polymerization experiments utilized a three-component
 504 dye/EDB/Iod system with concentrations set at 0.1%/2%/2% w/w/w. In contrast to prior
 505 experiments, our approach exhibited a substantial 20-fold reduction in the
 506 concentration of additives while maintaining a high monomer conversion.
 507 Simultaneously, the exposure time to sunlight was significantly curtailed, achieving

508 remarkable monomer conversions within just 70 s of sunlight irradiation, as opposed to
 509 the to 30 min required in earlier studies. In light of these findings and to the best of our
 510 knowledge [32, 33], B1, B2, B3, B10, and B11 represent the inaugural sunlight
 511 photoinitiators capable of utilizing additives at such minimal concentrations,
 512 concurrently achieving high monomer conversions within approximately one minute of
 513 sunlight exposure. This advancement positions these dyes at the forefront of solar
 514 photoinitiators in terms of efficiency and expeditious polymerization under sunlight.

515

516 **Table 5.** Acrylate function conversions obtained during the FRP of TMPTA at 405 nm
 517 and sunlight (30 min) using three-component photoinitiating dye/Iod/EDB (0.1%/2%/2%
 518 w/w/w) systems.

	Push-pull dyes	Absorption properties	Final Acrylate function conversion
Dye8 [34]		$\lambda_{\max} = 491 \text{ nm}$ $\epsilon_{\max} = 5330 \text{ M}^{-1} \cdot \text{cm}^{-1}$ $\epsilon_{405\text{nm}} = 3340 \text{ M}^{-1} \cdot \text{cm}^{-1}$	~91% (LED@405 nm, I = 110 mW.cm ⁻² , 400 s); ~88% (sunlight, 30 min)
CP7 [35]		$\lambda_{\max} = 689 \text{ nm}$ $\epsilon_{\max} = 113870 \text{ M}^{-1} \cdot \text{cm}^{-1}$ $\epsilon_{405\text{nm}} = 13640 \text{ M}^{-1} \cdot \text{cm}^{-1}$	~97% (LED@405 nm, I = 30 mW.cm ⁻² , 400 s); ~93% (sunlight, 30 min)
CP9 [35]		$\lambda_{\max} = 627 \text{ nm}$ $\epsilon_{\max} = 51700 \text{ M}^{-1} \cdot \text{cm}^{-1}$ $\epsilon_{405\text{nm}} = 4610 \text{ M}^{-1} \cdot \text{cm}^{-1}$	~98% (LED@405 nm, I = 30 mW.cm ⁻² , 400 s); ~91% (sunlight, 30 min)
CP11 [35]		$\lambda_{\max} = 671 \text{ nm}$ $\epsilon_{\max} = 47770 \text{ M}^{-1} \cdot \text{cm}^{-1}$ $\epsilon_{405\text{nm}} = 6560 \text{ M}^{-1} \cdot \text{cm}^{-1}$	~99% (LED@405 nm, I = 30 mW.cm ⁻² , 400 s); ~92% (sunlight, 30 min)

519 **5. Conclusion**

520 In this study, we synthesized and explored the potential of 15 new dyes based on
521 the 2-phenylnaphtho[2,3-*d*]thiazole-4,9-dione scaffold and 1 dye based on the 2,3-
522 diphenyl-1,2,3,4-tetrahydrobenzo[*g*]quinoxaline-5,10-dione scaffold as photoinitiators.
523 All dyes examined in this work have never previously been studied as photosensitizers
524 for photopolymerization processes. Particularly noteworthy is the fact that, despite the
525 synthesis of 2,3-diphenyl-1,2,3,4-tetrahydrobenzo[*g*]quinoxaline-5,10-diones being
526 reported in 1987, subsequent investigations into this family of dyes have been notably
527 sparse. Diverse photoinitiating systems were prepared by combining these dyes with
528 additives such as EDB and Iod. The strong absorption of these dyes exhibited in the
529 UV-visible region (> 400 nm) facilitated photopolymerization under the irradiation of
530 LED@405 nm and LED@450 nm. The proposed chemical mechanism was
531 corroborated using complementary techniques including steady-state photolysis,
532 fluorescence quenching experiments, cyclic voltammetry, and ESR-ST experiments.
533 Remarkably, B1, B2, B3, B10, and B11 emerged as successful photoinitiators for the
534 FRP of TMPTA under sunlight due to their excellent photoinitiation ability. Among
535 these, B10 exhibited the highest reactivity, achieving unprecedented monomer
536 conversions under sunlight, with FCs of 58% for TMPTA and 96% for PEGDA, all at
537 significantly low concentrations of photosensitizers and additives. These findings
538 position these dyes as promising candidates for the future development of efficient
539 sunlight photoinitiators. Finally, the three-component systems, B10/EDB/Iod and
540 B11/EDB/Iod, were successfully applied to 3D printing. In summary, the demonstrated
541 ability of these dyes to initiate polymerization under sunlight, coupled with their ease
542 of synthesis, rapid polymerization under both sunlight and artificial light sources, aligns
543 with the principles of green chemistry. These chromophores present a viable option for
544 large-scale industrial applications, such as exterior wall coatings, offering energy
545 efficiency and environmental sustainability in outdoor polymerization processes.

546

547

548 **Conflicts of interest**

549 The authors declare no competing financial interest.

550

551 **Acknowledgements**

552 This research project is supported by China Scholarship Council (CSC)

553 (No.202208220049).

554

555 **References**

- 556 1. Kaur; Manmeet; Srivastava; A.; K., *Journal of Macromolecular Science: Polymer*
557 *Reviews* **2002**, *42* (4), 481-481.
- 558 2. Corrigan, N.; Yeow, J.; Judzewitsch, P.; Xu, J.; Boyer, C., *Angew Chem Int Ed*
559 *Engl* **2019**, *58* (16), 5170-5189. DOI 10.1002/anie.201805473.
- 560 3. Zhang, Y.; Liu, Z.; Borjigin, T.; Graff, B.; Morlet-Savary, F.; Schmitt, M.; Gignes,
561 D.; Dumur, F.; Lalevée, J., *Green Chemistry* **2023**, *25* (17), 6881-6891. DOI
562 10.1039/d3gc02004e.
- 563 4. Mokbel, H.; Graff, B.; Dumur, F.; Lalevee, J., *Macromol Rapid Commun* **2020**, *41*
564 (15), e2000289. DOI 10.1002/marc.202000289.
- 565 5. Weems, A. C.; Delle Chiaie, K. R.; Yee, R.; Dove, A. P., *Biomacromolecules* **2020**,
566 *21* (1), 163-170. DOI 10.1021/acs.biomac.9b01125.
- 567 6. Zhou, A.; Xu, C.; Kanitthamniyom, P.; Ng, C. S. X.; Lim, G. J.; Lew, W. S.; Vasoo,
568 S.; Zhang, X.; Lum, G. Z.; Zhang, Y., *Adv Mater* **2022**, *34* (15), e2200061. DOI
569 10.1002/adma.202200061.
- 570 7. Khudyakov, I. V., *Progress in Organic Coatings* **2018**, *121*, 151-159. DOI
571 10.1016/j.porgcoat.2018.04.030.
- 572 8. Wang, S.-C.; Wu, Y.-H.; Hsieh, J.-B.; Ni, J.-S.; Chen, Y.-C., *Journal of*
573 *Photochemistry and Photobiology A: Chemistry* **2023**, *443*. DOI
574 10.1016/j.jphotochem.2023.114870.
- 575 9. Chen, L.; Kenkel, S. M.; Hsieh, P. H.; Gryka, M. C.; Bhargava, R., *ACS Appl*
576 *Mater Interfaces* **2020**, *12* (44), 50105-50112. DOI 10.1021/acsami.0c12158.
- 577 10. Abedin, F.; Ye, Q.; Spencer, P., *J Dent* **2020**, *99*, 103405. DOI
578 10.1016/j.jdent.2020.103405.
- 579 11. Xue, T.; Tang, L.; Tang, R.; Li, Y.; Nie, J.; Zhu, X., *Dyes and Pigments* **2021**, *188*.
580 DOI 10.1016/j.dyepig.2021.109212.
- 581 12. Fang, W. W.; Yang, G. Y.; Fan, Z. H.; Chen, Z. C.; Hu, X. L.; Zhan, Z.; Hussain,
582 I.; Lu, Y.; He, T.; Tan, B. E., *Nat Commun* **2023**, *14* (1), 2891. DOI
583 10.1038/s41467-023-38402-y.

- 584 13. Voll, D.; Barner-Kowollik, C., *Angewandte Chemie International Edition* **2013**,
585 52 (12), 3312-3312. DOI 10.1002/anie.201209688.
- 586 14. Liao, W.; Liao, Q.; Xiong, Y.; Li, Z.; Tang, H., *Journal of Photochemistry and*
587 *Photobiology A: Chemistry* **2023**, 435. DOI 10.1016/j.jphotochem.2022.114297.
- 588 15. Lee, Y.; Boyer, C.; Kwon, M. S., *Nature Reviews Materials* **2021**, 7 (2), 74-75.
589 DOI 10.1038/s41578-021-00409-6.
- 590 16. Fast, D. E.; Lauer, A.; Menzel, J. P.; Kelterer, A.-M.; Gescheidt, G.; Barner-
591 Kowollik, C., *Macromolecules* **2017**, 50 (5), 1815-1823. DOI
592 10.1021/acs.macromol.7b00089.
- 593 17. Li, J.; Zheng, H.; Lu, H.; Li, J.; Yao, L.; Wang, Y.; Zhou, X.; Nie, J.; Zhu, X.; Fu,
594 Z., *European Polymer Journal* **2022**, 176. DOI 10.1016/j.eurpolymj.2022.111393.
- 595 18. Bella, F.; Sacco, A.; Salvador, G. P.; Bianco, S.; Tresso, E.; Pirri, C. F.;
596 Bongiovanni, R., *The Journal of Physical Chemistry C* **2013**, 117 (40), 20421-
597 20430. DOI 10.1021/jp405363x.
- 598 19. Ye, S.; Shi, W.; Liu, Y.; Li, D.; Yin, H.; Chi, H.; Luo, Y.; Ta, N.; Fan, F.; Wang, X.;
599 Li, C., *J Am Chem Soc* **2021**, 143 (32), 12499-12508. DOI 10.1021/jacs.1c00802.
- 600 20. Winther-Jensen, O.; Armel, V.; Forsyth, M.; MacFarlane, D. R., *Macromolecular*
601 *Rapid Communications* **2010**, 31 (5), 479-483. DOI 10.1002/marc.200900701.
- 602 21. Zhao, Y.; Ding, C.; Zhu, J.; Qin, W.; Tao, X.; Fan, F.; Li, R.; Li, C., *Angew Chem*
603 *Int Ed Engl* **2020**, 59 (24), 9653-9658. DOI 10.1002/anie.202001438.
- 604 22. Schmitt, M., *Nanoscale* **2015**, 7 (21), 9532-44. DOI 10.1039/c5nr00850f.
- 605 23. Hammoud, F.; Hijazi, A.; Duval, S.; Lalevee, J.; Dumur, F., *European Polymer*
606 *Journal* **2022**, (162-), 162.
- 607 24. Mokbel, H.; Noirbent, G.; Gimes, D.; Dumur, F.; Lalevee, J., *Beilstein J Org*
608 *Chem* **2021**, 17, 2067-2076. DOI 10.3762/bjoc.17.133.
- 609 25. Abdallah, M.; Dumur, F.; Graff, B.; Hijazi, A.; Lalevée, J., *Dyes and Pigments*
610 **2020**, 182. DOI 10.1016/j.dyepig.2020.108580.
- 611 26. Fouassier; JeanPierre, *Wiley-VCH* **2012**.
- 612 27. Romańczyk, P. P.; Kurek, S. S., *Electrochimica Acta* **2017**, 255, 482-485.

- 613 28. Yu, Z.; Su, J.; Huang, C.; Wei, J.; Han, L.; Ye, Q.; Li, Y., *Asian Journal of Organic*
614 *Chemistry* **2022**.
- 615 29. Haug, J.; Scheffler, K.; Stegmann, H. B.; Vonwirth, S.; Wei, J. E.; Conzelmann,
616 W.; Hiller, W., *European Journal of Inorganic Chemistry* **1987**, 120 (7), 1125-1132.
- 617 30. Han, W.; Shi, Y.; Xue, T.; Wang, T., *Dyes and Pigments* **2019**, 166, 140-148. DOI
618 10.1016/j.dyepig.2019.03.023.
- 619 31. Lalevée, J.; Gigmes, D.; Bertin, D.; Graff, B.; Allonas, X.; Fouassier, J. P.,
620 *Chemical Physics Letters* **2007**, 438 (4-6), 346-350. DOI
621 10.1016/j.cplett.2007.03.029.
- 622 32. Tehfe, M.; Louradour, F.; Lalevée, J.; Fouassier, J.-P., *Applied Sciences* **2013**, 3
623 (2), 490-514. DOI 10.3390/app3020490.
- 624 33. Dumur, F., *Eur. Polym. J.* **2023**, 189, 111988-112008.
- 625 34. Sun, K.; Liu, S.; Pigot, C.; Brunel, D.; Graff, B.; Nechab, M.; Gigmes, D.; Morlet-
626 Savary, F.; Zhang, Y.; Xiao, P.; Dumur, F.; Lalevée, J., *Catalysts* **2020**, 10 (10).
627 DOI 10.3390/catal10101196.
- 628 35. Sun, K.; Pigot, C.; Zhang, Y.; Borjigin, T.; Morlet-Savary, F.; Graff, B.; Nechab,
629 M.; Xiao, P.; Dumur, F.; Lalevée, J., *Macromolecular chemistry and physics* **2022**,
630 (4), 223.
- 631